Energy and Exergy Analysis and Optimization of a Pentageneration (Cooling, Heating, Power, Water and Hydrogen)

Norouzi, Nima
Department of Energy Engineering and Physics, Amirkabir University of Technology, Tehran, I.R. IRAN

Alireza, Bozorgian*+
Department of Chemical Engineering, Mahshahr Branch, Islamic Azad University, Mahshahr, I.R. IRAN

ABSTRACT: *The proposed poly-generation plant, which generates power, cooling, and freshwater, consists of five subsystems. A Solid Oxide Fuel Cell (SOFC) plant generates electricity using CH_4 as fuel. Steam Reforming happens in the anode to generate the required H_2 for the electrochemical process. The thermal energy of these processes enhances the exhaust gas temperature from the solid oxide fuel cell plant, which can be reused using a Kalina cycle and humidification-dehumidification-RO desalination plants. This exhaust gas from the afterburner of a solid oxide fuel cell evaporates the ammonia-water mixture in a Kalina cycle and preheats the feedwater to be entered in the humidifier of the desalination unit. There has been an evaluation of the effect of various system parameters such as turbine inlet temperature, compressor pressure ratio, carbon dioxide to methane molar ratio, steam generator temperature, and mass flow ratio of the desalination system on overall system performance. Also, single- and multi-objective optimization methods have been used to optimize the general system compared to the base model.*

KEYWORDS: *Cogeneration; Genetic optimization; Hydrogen industry; Absorption refrigeration; Pentageneration.*

INTRODUCTION

More than ever, developing cost-effective, reliable, sustainable, and secure power generation systems has become increasingly important as global energy demand continues to grow with population growth and rising living standards. Energy supply is a global problem when conventional fossil and nuclear fuel resources are concentrated in a limited number of geographical areas worldwide. At the same time, many other countries rely heavily on fuel imports. Power generation requires a multidimensional solution that can simultaneously overcome the needs for higher efficiency, less pollution, the use of a wide variety of energy sources, etc. In recent years, multiple energy generation systems have emerged as a powerful solution to these problems. These systems operate as integrated systems and can be composed of several subsystems, such as power generation cycles, hydrogen production systems, refrigeration cycles, freshwater production

**To whom correspondence should be addressed.*
+ E-mail: a.bozorgian@mhriau.ac.ir
1021-9986/2023/7/2355-2371 17/$/6.07

systems, and home heating systems[1].

Given the importance of energy conversion issues globally, using energy resources and the waste heat recovery industry can be a good way to increase multiple energy production systems[2]. In recent years, interest in using waste heat recovery has seriously increased, and researchers have proposed new methods for generating power through high and medium-temperature heat sources. Among the methods proposed for power cycles, the Gas Turbine Cycle - Modular Helium Reactor (GT-MHR) cycle due to its important features and characteristics such as less environmental pollution, economic cost, high reactor power, and also The high flow temperature of the gas turbine outlet can be used as a suitable high-temperature source (above 500 ° C) and the base cycle in combination with other systems. In one example of a gas turbine modular helium reactor cycle, about 300 MW of thermal energy is wasted in the pre-cooler to minimize compressor consumption[3,4]. Due to the amount of heat lost in this part of the system, a combination of several systems can be used in connection with the base cycle (gas turbine cycle - modular helium reactor). Many studies have been used to recover the lost heat from the gas turbine outlet flow and use it as a suitable heat source to supply power generation, cooling and heating systems, etc. [5].

Astolfi et al. first proposed using Organic Rankine Cycles (ORC) to recover heat loss from the gas turbine-modular helium reactor cycle and power generation. Their results showed that the efficiency of the first law of the hybrid system increases by about 10.1-5.1% compared to the base cycle[6]. In another study, *Zhai et al*. studied the heat dissipation application of a gas turbine system-modular helium reactor with a two-stage compressor as heat sources in two organic Rankin cycles. They concluded that the efficiency of the first and second laws of the case system Comments increased by 3%[7].

Orhan and Babu presented and analyzed heat loss recovery of the base cycle to produce power and pure water. Their results also showed that for every 50 ° C increase in turbine inlet temperature, energy efficiency increases by 2.5-4%, and pure water production rate decreases by 6.5%[8]. In another study, *Zhong et al*. investigated the heat lost in the base cycle for power generation and cooling using the ammonia-water cycle. They concluded that the efficiencies of the first and second laws increased 9-15 and 4-10%, respectively[9]. Also, in the continuation of the research of this combined system, they studied the economic exergy of the system, and the results showed that the unit cost of the combined system is reduced by 4.5% compared to the base cycle[10-24].

The application of different arrangements of organic Rankin cycles and ejector refrigeration to recover the lost heat of the base cycle was presented by *Han et al*. [25]. They also evaluated the combined system and concluded that the highest exergy efficiency was about 49.69%, 2% higher than the base cycle. Another study modeled thermodynamics and compared two systems combined with a base cycle (MHR/NH_3-Water) suitable for the first and second laws of thermodynamics[26]. Also, the mass flow of helium in the combined Rankin organic cycle system is lower than in the combined water-ammonia cycle. *Cao et al*. investigated the combined system of simultaneous production of modular helium gas turbine, Kalina cycle, and absorption refrigeration cycle from the energy and exergy economy perspective. Their simulations showed that in the input cycle of the base cycle, the net power is 304462 kW, the total irreversibility is 289976 kW, and the exergy efficiency of the total co-production cycle is 68.9%[27].

Thermoeconomic analysis evaluated a new system combining the gas turbine-modular reactor cycle, the water-ammonia absorption power cycle, and the Liquefied Natural Gas (LNG) cooling system. It concluded that in the case of Optimally, the highest net output power and the lowest exergy destruction rate of the system are 383 and MW467[28].

The research proposed a combined system of hydrogen production and a gas turbine cycle-modular helium reactor. In this system, water electrolysis produces hydrogen, which breaks down water molecules into hydrogen and oxygen through heat recovered from the base cycle. The results showed that hydrogen production and base cycles increased energy efficiency by about 50%[29].

Other researchers also produced hydrogen simultaneously through the electrolysis of water and power using nuclear power plants and concluded that hydrogen production costs about \$ 2 H_2/Kg[30]. Another study performed energy analysis and exergy of hydrogen production by combining organic Rankine cycles, base cycle, and electrolysis system (PEM). The results showed that by increasing the pressure ratio of the base cycle compressor, the exergy efficiency of the hybrid system is increased, and also the rate of hydrogen production

increases with increasing the inlet temperature of the helium gas turbine. In optimal conditions, the highest exergy efficiency and hydrogen production rates are 49.21% and 56.2 kg/h, respectively[31]. Another study proposed a combined freshwater production system using dissipated heat recovery in a gas turbine-modular helium reactor cycle[32].

The results showed that freshwater production costs are reduced by about 34% compared to conventional desalination systems. Some researchers investigated the thermodynamic analysis of two reverse osmosis membrane process systems for freshwater production and the base cycle. The heat required for the desalination system is provided by recycling the base cycle heat. The results showed that the exergy efficiency of the hybrid system increases by about 10% and reaches 41%[32-34].

In another study, researchers developed an Artificial Neural Network (ANN)--based data-driven model using 485,710 actual operation datasets for optimizing the SMR process. Data preprocessing was performed to improve the data quality, including outlier removal and noise filtering. A model with high accuracy (average R2 = 0.9987) was developed, which can predict six variables through hyperparameter tuning of a neural network model, as follows: syngas flow rate; CO, CO_2, CH_4, and H_2 compositions; and steam temperature. During optimization, the search spaces for nine operating variables, namely the natural gas flow rate for the feed and fuel, the hydrogen flow rate for desulfurization, water flow rate and temperature, airflow rate, SMR inlet temperature, and pressure, and Low-Temperature Shift (LTS) inlet temperature, were defined and applied to the developed model for predicting the thermal efficiencies for 387,420,489 cases. Subsequently, five constraints were established to consider the feasibility of the process, and the decision variables with the highest process thermal efficiency were determined. The process operating conditions showed a thermal efficiency of 85.6%[35-50].

The main objective of this study paper is to study the integration of this system with a Combined Cooling, Heating, and Power cycle comprised of a gas turbine, an organic Rankine cycle, and an absorption refrigeration system. Energy and exergy analyses are applied to the system and the effect of key parameters on the system performance are analyzed.

The results show that under design conditions, the system can generate 33.67 kW of electricity, 2.56 kW of cooling, and 1.82 ton per day of hot water with a round-trip energy efficiency of 53.94%. Also, exergy analysis reveals that wind turbines, combustion chambers, and compressed air storage systems have the highest amount of exergy destruction respectively. Finally, sensitivity analysis shows that parameters related to gas turbines are the most prominent parameters of the system which can change the performance of the system considerably [51].

In a study, a hybrid system composed of a gas turbine, an ORC cycle, and an absorption refrigeration cycle is proposed as a combined cooling, heating, and power system for residential usage. Thermodynamic analysis is applied to the system. Also, a parametric analysis is carried out to investigate the effect of different parameters on the system performance and output cooling, heating, and power. The results show that under design conditions, the proposed plant can produce 30 kW of power, 8 kW of cooling, and almost 7.2 tons of hot water with an efficiency of 67.6%. Moreover, parametric analysis shows that pressure ratio and gas turbine inlet temperature are the most important and influential parameters. After these two, ORC turbine inlet temperature is the most effective parameter as it can change both the net output power and energy efficiency of the system[52].

Another study attempts to go beyond the conventional framework of the integrated solar transcritical CO2 power cycle works, aimed at further utilization of available exergy as much as possible. This paper proposed a novel system for hydrogen and freshwater production in which a Stirling engine is used instead of a condenser, for the places with abundant access to solar radiation and sea, and least to freshwater sources. This proposal leads to further utilization of streams' exergy through the system instead of wasting to the environment, and further power production by the engine followed by the higher products[53].

A novel solar power, water, and hydrogen cogeneration plant with recovery of cryogenic energy is proposed in this study to produce hydrogen and permeate water by gasification of Liquefied Natural Gas (LNG). A mathematical model is developed to simulate the system and an exergy and thermodynamic parametric analysis is carried out to investigate the effect of several thermodynamic parameters on overall system performance. A dynamic Reverse Osmosis (RO) desalination model is introduced

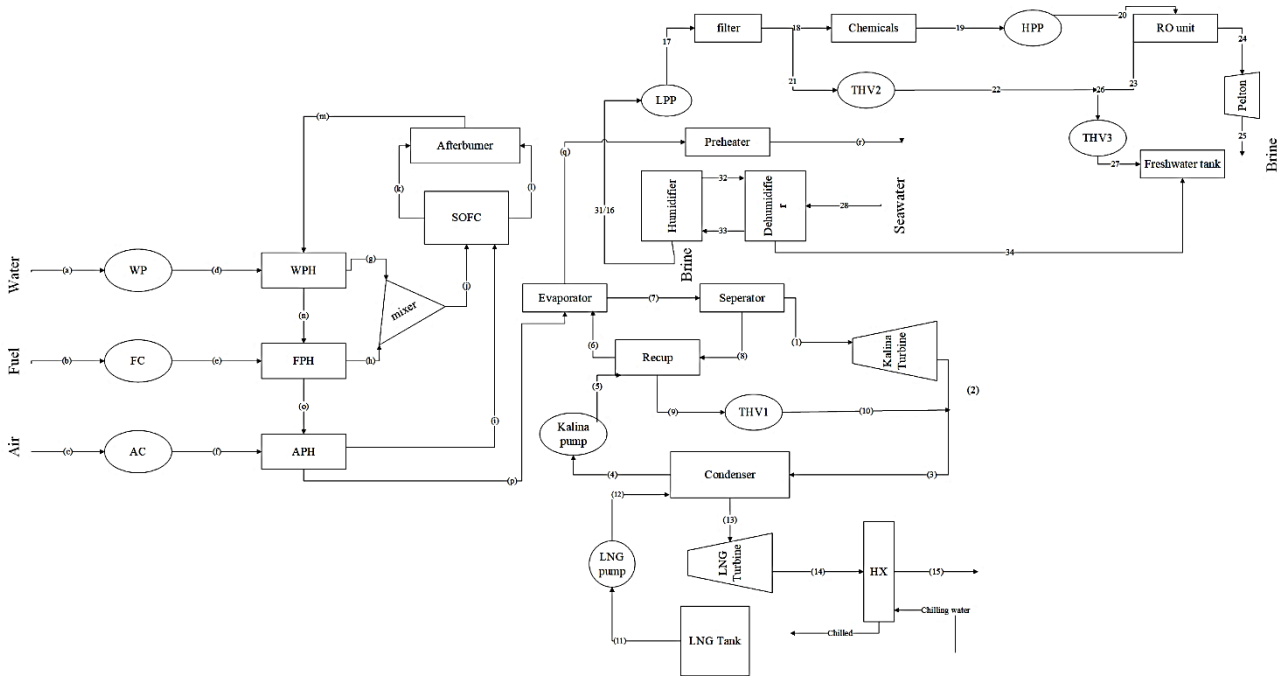

Fig. 1: The schematic of the proposed poly-generation system

to produce different permeate and feed water mass flow rates. By the results, about 26.8% of the net produced power is recovered by a turbine located in RO brine discharge[54].

In a paper, a novel CO_2 transcritical power cycle that is driven by solar energy integrated by a cryogenic LNG recovery unit is investigated. In the proposed cycle, the condenser unit of the CO_2 power cycle is replaced by a Stirling engine. Thermodynamic and exergy analyses are carried out to evaluate the performance of the presented system. Furthermore, in order to investigate the impact of the utilization of Stirling engines instead of conventional condenser units, the proposed cycle is compared with the typical CO_2 power cycle. The results show that employing the Stirling engine decreases the exergy destruction from 17% in the typical cycle to 8.85%. In addition, the total generated power of the novel system is considerably boosted by about 15 kW in off-peak times and more than 20 kW in the peak time. Moreover, the integration of the Stirling engine also decreases LNG mass flow rate. Therefore, the required heat exchanger area in the LNG heater is also lowered [55-67].

In recent years, significant research has been conducted on heat recovery from the modular gas turbine helium reactor cycle and its combination with various energy systems. A comprehensive study of energy and exergy analysis on multiple energy production and the combination of different systems has not been done on a pentageneration cycle, so due to limited fossil fuel resources and renewable energy sources, the idea of producing multiple products at the same time is both economically viable and more energy-efficient. In this study, to increase the efficiency of the base cycle, the use of wasted heat and multiple energy production, the combination of the base cycle (power generation) with hydrogen production system, absorption refrigeration cycle, desalination system, and home heating systems have been used. The objectives of this research include:

1. Introducing a new system of multiple energy production using a gas turbine cycle - modular helium reactor
2. Comprehensive modeling of the proposed thermodynamics of the system
3. Comprehensive parametric study to investigate the effect of different parameters on the performance of the hybrid system
4. Optimization of thermodynamic conditions using the genetic algorithm to determine the combined system's maximum energy efficiency and exergy.

EXPERIMENTAL SECTION

Conceptual model

The proposed poly-generation plant, which generates

power, cooling, and freshwater, consists of five subsystems (shown in Fig. 1). A solid oxide fuel cell (SOFC) plant generates electricity using CH_4 as fuel. Steam Reforming happens in the anode to generate the required H_2 for the electrochemical process. The thermal energy of these processes enhances the exhaust gas temperature from the solid oxide fuel cell plant, which can be reused using a Kalina cycle and humidification-dehumidification-RO desalination plants. This exhaust gas from the afterburner of a solid oxide fuel cell evaporates the ammonia-water mixture in a Kalina cycle and preheats the feedwater to be entered in the humidifier of the desalination unit.

The operating fluid in the Kalina cycle is a constant mixture of water and ammonia. However, the fluid's mass ratio varies during the processes of this plant because of the separator. Primarily, the recovered thermal energy from solid oxide fuel cells enhances the ammonia-water fluid's temperature in the Kalina cycle's evaporator. After that, the ammonia part is separated from the water fraction in a separator to generate power using a Kalina turbine. Also, the fluid separated in the separator transfers its heat to the output cold mixture of the Kalina pumping system in a recuperator unit. Then, the two separated fractions are mixed again, and transfer their remnant of heat to the liquified natural gas cold stream in the condenser. This should be considered that the total mass of ammonia-water is always fixed in the KC, and just mass fractions vary during the process. Thus the composition of the fluid never changes, and the unit is always steady. The generated cooling load in this cycle is potentially utilized for local uses.

In contrast, the power produced by the turbine, solid oxide fuel cell, and Kalina turbine is injected into the grid, and a part is used in the RO desalination unit. The turbines of the plant also generate the needed power for the pumps. Briefly, the solid oxide fuel cell unit produces the needed electricity for compressors and pumps, and excess power is directed to the grid.

Mathematical model

In this paper, mathematical models and thermodynamic investigations are needed to study the energy and exergy performances of the proposed poly-generation plant. This model is being made taking the steady-state condition, negligible pressure drops and losses of heat in the pipes, and inconsiderable variations of the potential and kinetic energies into account as the main simplification assumptions.

Solid oxide fuel cell unit

As the Solid oxide fuel cell uses H_2 as the main fuel, CH_4 is fed to the steam reformer system. CH_4 is reformed to hydrogen in this steam-reforming process, as illustrated in Equation (1), respectively. Then, power is produced in the solid oxide fuel cell by hydrogen oxidation (As equation (2) shows).

$$Methane + water \leftrightarrow Hydrogen + Carbon\ monoxid \quad (1)$$

$$Hydrogen + Oxygen \leftrightarrow Water \quad (2)$$

The generated power of the solid oxide fuel cell is calculated in Equation (3):

$$W_{FC} = iA_{act}N_{cell}V_{cell} \quad (3)$$

In this Equation, i stands for the current density, N_{cell} for several cells, A_{act} for activation area, and V_{cell} for the voltage of the cell. Equation (4) represents V_{cell} estimation using the reversible voltage presented by V_N and voltage losses of V_{loss}.

$$V_{cell} = V_N - V_{loss} \quad (4)$$

$$V_{loss} = \zeta_{ohm} + \zeta_{act} + \zeta_{conc} \quad (5)$$

Also in Equation (5), ζ_{ohm}, ζ_{act}, and ζ_{conc} stands for the ohmic, activation, and concentration overpotentials, respectively.

Kalina cycle unit

As mentioned above, the heat output from the Solid oxide fuel cell unit is first recovered by the Kalina cycle and then by the desalination unit. In the first stage, the operating fluid Kalina cycle unit (ammonia-water) evaporates as the Equation (6):

$$m_G(h_p - h_q) = m_6(h_7 - h_6) \quad (6)$$

The m_G stands for the mass flow rate of the solid oxide fuel cell. Following separating the mixture in the separator (as shown in Equations (7) and (8)), power can be generated in the turbine (see Equation (9)).

$$m_7h_7 = m_8h_8 + m_1h_1 \quad (7)$$

$$m_7X_7 = m_8X_8 + m_1X_1 \quad (8)$$

$$W_{tur} = m_1(h_1 - h_2) \quad (9)$$

The separated liquid flows to the recuperator and gives the thermal energy to the mixture pumped from the condenser as Equation (10) states:

$$m_8(h_9 - h_8) = m_5(h_6 - h_5) \quad (10)$$

This operating liquid then flows through THV1 plant (as shown in Equation (11)) and then mixes again with the turbine outlet (as shown Equation (12)).

$$h_9 = h_{10} \quad (11)$$

$$m_2h_2 + m_{10}h_{10} = m_3h_3 \quad (12)$$

The condenser uses the waste heat from the fluid in the LNG stream as a low-temperature heat exchanger as shown in Equation (13):

$$m_3(h_4 - h_3) = m_{11}(h_{13} - h_{12}) \quad (13)$$

Finally, the fluid is pumped again to enhance the pressure and reach the evaporator as can be seen in Equation (14):

$$W_{pump} = m_4(h_5 - h_4) \quad (14)$$

Liquied natural gas plant

The Liquied natural gas pressure is enhanced by the LNG pump (as shown in Equation (15)) to pass through the Kalina cycle condenser and become gaseous (as seen in Equation (13)).

$$W_{LNG,Pump} = m_{11}(h_{12} - h_{11}) \quad (15)$$

The turbine used can generate more power for the RO unit as Equation (16) shows:

$$W_{LNG,tur} = m_{11}(h_{14} - h_{13}) \quad (16)$$

The LNG output cooling capacity can be obtained through the cooling plant as shown in Equation (17):

$$Q_{cooling} = m_{11}(h_{15} - h_{14}) \quad (17)$$

Desalination unit

The primary components of the desalination plant are heater, humidifier, dehumidifier and RO system. The heater (as seen in Equation (18)) transfers the heat of the operating fluid, when the mass and energy transfer occurs in the humidifier (see Equation (19)) and the dehumidifier (see Equation (20)).

$$Q_H = m_{30}h_{30} - m_{29}h_{29} \quad (18)$$

$$m_{31}h_{31} - m_{30}h_{30} = m_{da}(h_{33} - h_{32}) \quad (19)$$

$$m_{29}h_{29} - m_{28}h_{28} + m_{34}h_{34} = m_{da}(h_{32} - h_{33}) \quad (20)$$

m_{da} stands for the mass flow of dry air. Based on the output heat content to the heat obtained through heat transfer in the heater, the output ratio (GOR) can be calculated as equation (21) states:

$$GOR = \frac{m_{34}h_{f9}}{Q_H} \quad (21)$$

Where the h_{f9} is the latent heat of water evaporation. Among the existing desalination plants, which are powered by electrical energy, reverse osmosis plants have a bright future and promising performance. Due to the y_s as the mass fraction of salt, salinity of brine and freshwater are calculated by equations (22) and (23):

$$m_{20}y_{s,20} = m_{23}y_{s,23} + m_{24}y_{s,24} \quad (22)$$

$$m_{23}y_{s,23} = m_{22}y_{s,22} + m_{26}y_{s,26} \quad (23)$$

The plant recovery ratio or ratio of fresh water to feed-in water is considered as Equation (24):

$$R_r = \frac{m_{product}}{m_{feed-in}} = \frac{m_{27}}{m_{25}} \quad (24)$$

Furthermore, Equation (25) estimates the bypass mass rate considering the mass balance in the mixer:

$$m_{21} = m_{26}\left(\frac{y_{s,26} - y_{s,23}}{y_{s,21} - y_{s,23}}\right) \quad (25)$$

Exergy equations

An exergy analysis is a very useful to understand the performance of components of each system in an integrated performance and their ability to produce corelative impacts. In this sense, ex_{ch} stands for chemicals exergy and ex_{ph} for the physical exergies which must be determined. Then the exergy destruction can be calculated using the exergy equilibrium equations as seen in Table 1. For a given substance, the ex is exergy which can be calculated as Equation (26):

$$ex = e_{ch} + ex_{ph} \quad (26)$$

The physical exergy (As shown in Equation (27)) shows that the maximum physical work potential that can be achieved by capturing the mass flow in thermomechanical equilibrium with the environment while obtaining the chemical exergy is dependent on the mass fraction of Kalina operating fluid (As seen Equation (28)).

Table 1: Exergy input and output values for different components of the integrated system

Unit	Exergy equilibrium equation
FCG	
SOFC	$Ex_j^{ch} + Ex_j^{ph} + Ex_i^{ch} + Ex_i^{ph} = Ex_k^{ch} + Ex_k^{ph} + Ex_l^{ch} + Ex_l^{ph} + Ex_{D,SOFC}$
AC	$Ex_c + W_{AC} = Ex_f + Ex_{D,AC}$
FC	$Ex_b + W_{FC} = Ex_e + Ex_{D,FC}$
WP	$Ex_a + W_{WP} = Ex_d + Ex_{D,pum}$
AP	$Ex_o + Ex_f = Ex_p + Ex_i + Ex_{D,AP}$
FP	$Ex_n + Ex_e = Ex_h + Ex_o + Ex_{D,FP}$
WP	$Ex_m + Ex_d = Ex_g + Ex_n + Ex_{D,WP}$
Mix	$Ex_g + Ex_h = Ex_j + Ex_{D,mix}$
AB	$Ex_k + Ex_l = Ex_m + Ex_{D,AB}$
KC	
EVA	$Ex_p + Ex_6 = Ex_q + Ex_7 + Ex_{D,EVA}$
SEP	$Ex_7 = Ex_1 + Ex_8 + Ex_{D,SEP}$
TUR	$Ex_1 = Ex_2 + Ex_{Tur} + Ex_{D,Tur}$
RECUP	$Ex_8 + Ex_5 = Ex_9 + Ex_6 + Ex_{D,RECUP}$
THV1	$Ex_9 = Ex_{10} + Ex_{D,THV1}$
Pum	$Ex_4 + W_{pump} = Ex_5 + Ex_{D,pum}$
WH	$Ex_3 + Ex_{12} = Ex_4 + Ex_{13} + Ex_{D,con}$
LNGC	
Tur	$Ex_{13} = Ex_{14} + W_{Tur} + Ex_{D,Tur}$
CU	$Ex_{13} = Ex_{14} - Ex_{Q,vap} + Ex_{D,con}$
Pum	$Ex_{11} + W_{pum} = Ex_{12} + Ex_{D,pum}$
HDH-RO	
HUM	$Ex_{30} + Ex_{33} = Ex_{31} + Ex_{32} + Ex_{D,HUM}$
DHUM	$Ex_{32} + Ex_{28} = Ex_{33} + Ex_{29} + Ex_{D,DHUM}$
ROM	$Ex_{20} = Ex_{23} + Ex_{24} + Ex_{D,RO}$
LPP	$Ex_{16} + W_{LPP} = Ex_{17} + Ex_{D,LPP}$
HPP	$Ex_{19} + W_{HPP} = Ex_{20} + Ex_{D,HPP}$
PTu	$Ex_{24} = Ex_{25} + W_{PTU} + Ex_{D,PTU}$
THV2	$Ex_{21} = Ex_{22} + Ex_{D,\mathrm{THV2}}$
THV3	$Ex_{26} = Ex_{27} + Ex_{D,\mathrm{THV3}}$

$$ex_{ph} = (h - h_0) + T_0(s - s_0) \quad (27)$$

$$ex_{ch} = \left[\frac{e_{ch}^{-0},NH_3}{M_{NH_3}}\right] y + \left[\frac{e_{ch}^{-0},H_2O}{M_{H_2O}}\right] \quad (28)$$

Equation (29) provides the share of the k_{th} component in the overall exergy destruction rate.

$$Y_k^* = \frac{Ex_{D,k}}{Ex_{D,tot}} \quad (29)$$

Finally, the total performance must be estimated to determine the efficiency of the system and compare it with other suggested plants (see Equations (30) and (31)).

$$\eta_{en} = \frac{W_{grid} + Q_{cooling} + m_{freshwater} h_{freshwater}}{Q_{in}} \quad (30)$$

$$\eta_{ex} = \frac{W_{grid} + Ex_{cooling} + Ex_{freshwater}}{Ex_{in}} \quad (31)$$

Optimization method

Using the following algorithm called firefly, the optimum point of the decision parameters is calculated (see Fig. 2).

{"Objective function f(x), x=(x1,…, xd)T
Generate initial population of fireflies xi (i=1, 2, 3,.., n
Light intensity Ii at Xi is determined by f(xi)
Define light absorption coefficient γ
While (t<maxGeneration)
For i=1; n all n fireflies
For j=1; I all n fireflies
If (Ij>Ii), move firefly i towards j in d-dimension; end if
Attractiveness varies with distance r via exp[-γr]
Evaluate new solutions and update light intensity
End for j
End for i
Rank the fireflies and find the current best
End while
Post-process results and visualization."
The Pseudocode of the firefly optimization Algorithm (FO)}

The optimization method is implemented on the plant using the mentioned algorithm. This method includes Exergy efficiency, energy efficiency, and other technical parameters of the condensing system (see Table 2). Moreover, the results of this optimization are compared with other studies that implemented a Genetic Algorithm (GA) (see table 3). The validation in this study is done by comparing the results of the simulation with other papers. The results are compared to the results of the *Abbassi et al*. to compare the results of the FO optimization process with the other optimization algorithms (GA).

RESULTS AND DISCUSSION

Data validation

This section compares the modeling results for each subsystem with several sources in Table 3[19, 25, 36]. For the hydrogen production subsystem, the conversion percentage of methane and carbon dioxide and the amount of hydrogen production have been validated by *Abbassi et al*. in the molar ratio of water vapor to carbon equal to 1.32, the molar ratio of carbon dioxide to methane equal to 0.98[45]. Also, the results of performance parameters of gas turbine system - modular helium reactor and absorption

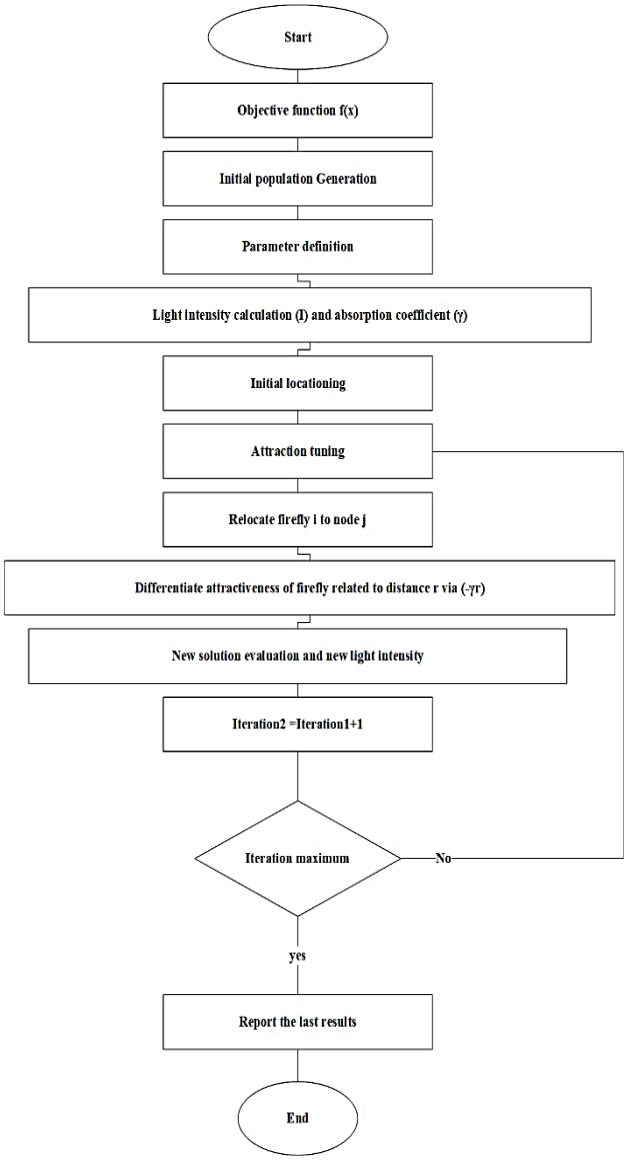

Fig. 2: Firefly Algorithm schematics

refrigeration cycle have been validated by *Abbassi et al.* [19]. The results show a good agreement between the parameters calculated in the present work and valid sources.

Results

According to the optimization methods mentioned in the previous section and considering the range of thermodynamic variables in Table 1, the optimal performance parameters of the energy analysis and exergy of the system are presented in Table 4. Decision variables and objective functions are compared with the baseline model. According to the results obtained in the multi-objective optimization method, the energy efficiency and exergy of the multiple production systems compared to the base model have been improved by 1.57 and 0.7%, respectively, and reached 74.41 and 50.21%, respectively. Other results from other optimization methods are shown in Tables 4-6.

Table 2: Optimization variables considered in the optimization process

Variable	Range	Variable	Range
T_j	[850-950]	S/C	[2.0-3.0]
A_{act}	[0.005-0.015]	T_{11}	[90-130]
$PPTD_{KC,Recup}$	[6-30]	P_{11}	[60-120]
W/A	[2.2-2.4]	r_{LNG}	[9-15]
TTD_{Heater}	[4-20]	$PPTD_{Con}$	[6-30]
T_{28}	[295.6-301.2]	TTD_{Con}	[6-30]
		A/W	[0.5-0.8]

Table 3: Simulation results compared with the results [19]

Variable	This paper	Abbassi et al.	Error
T_j	897.29	900	0.3%
A_{act}	0.01	0.01	0.0%
$PPTD_{KC,Recup}$	9.82	10	1.8%
W/A	2.26	2.333	3.1%
TTD_{Heater}	4.93	5	1.4%
T_{28}	297.28	298.15	0.3%
S/C	2.5	2.5	0.0%
T_{11}	113.31	111.15	1.9%
P_{11}	101.05	101.325	0.3%
r_{LNG}	11.82	25	1.5%
$PPTD_{Con}$	24.1	25	3.6%
TTD_{Con}	24.85	25	0.6%
A/W	0.72	0.7	2.9%

Table 5 shows the values of exergy destruction, exergy destruction ratio, and exergetic efficiencies in various optimal modes for each component of the overall system compared to the baseline model. According to the optimal mode types for each component, the share of reactor exergy destruction due to heat transfer and internal nuclear reactions is the highest. In the multi-objective optimization model, the base mode value is reduced to 1.38%. Also, the exergy destruction of the whole system in the multi-objective optimization model has been reduced by 0.74% compared to the base model.

Table 4: Optimum and technical inputs estimated for calculation of final results

Parameter		Parameter	
T_j	897.29	S/C	2.5
FUF	84.38	η_{FC}	84.67
i	5534.89	η_{AC}	85.06
A_{act}	0.01	ΔP_{SOFC}	2.01
N_{cell}	54692.12	ΔP_{HX}	1.98
N_e	2.01	ΔP_{AB}	3.03
$i_{exc,an}$	6478.46	T_{11}	113.31
$i_{exc,ca}$	2524.86	P_{11}	101.05
Dif_{an}	1.90E-05	r_{LNG}	11.82
Dif_{ca}	4.90E-06	$PPTD_{Con}$	24.1
t_{an}	4.90E-05	TTD_{Con}	24.85
t_{ca}	5.20E-05	A/W	0.72
t_{ele}	1.07E-03	P_1	3018.55
t_{int}	2.90E-03	T_7	384.3
T_4	292.57	$\eta_{KC,Tur}$	85.38
$PPTD_{KC,Recup}$	9.82	$\eta_{KC,pum}$	75.18
η_{HPP}	90.53	$\eta_{Pelton,Tur}$	79.53
η_{LPP}	87.2	RRO	0.55
MSR	0.98	T_{28}	297.28
FWS	34850.02	T_{30}	353.81
W/A	2.26	TTD_{Heater}	4.93
T_{31}	299.04	η_{DHUM}	84.28
η_{HUM}	84.4	ω_a	93

Table 5: Optimized results of the Energy analysis

State	T (K)	P (kPa)	n (mol/s)	Mole fraction percentage						
				CH_4	H_2O	H_2	CO	CO2	O_2	N_2
a	298.09	101.16	6.46	0	100	0	0	0	0	0
b	298.09	101.16	2.44	100	0	0	0	0	0	0
c	298.09	121.76	194.65	0	0	0	0	0	21.5	78.5
d	298.09	121.8	6.46	0	100	0	0	0	0	0
e	312.35	121.8	2.44	100	0	0	0	0	0	0
f	313.51	118.63	194.65	0	0	0	0	0	20.61	79.39
g	900.26	118.63	6.46	0	100	0	0	0	0	0
h	900.26	118.63	2.44	100	0	0	0	0	0	0
i	900.26	118.63	194.65	0	0	0	0	0	20.78	79.22
j	900.26	115.83	8.86	27.8	72.2	0	0	0	0	0
k	955.86	115.83	14.08	0	71.17	10.69	1.44	16.7	0	0
l	955.86	113.11	191.62	0	0	0	0	0	19.4	80.6
m	1015.75	110.99	203.24	0	5.63	0	0	1.29	17.6	75.48
n	943.42	108.12	203.24	0	5.63	0	0	1.29	17.6	75.48
o	934.05	106.14	203.24	0	5.63	0	0	1.29	17.6	75.48
p	394.23	106.14	203.24	0	5.63	0	0	1.29	17.6	75.48
q	383.75	106.14	203.24	0	5.63	0	0	1.29	17.6	75.48

Table 6: Optimized results of the energy analysis

	Fluid Composition	T(K)	P(kPa)	Ex(kW)	m(kg/s)
1	A/W=98.9%	367.32	2983.3	1064.87	0.054
2	A/W=98.9%	319.14	1094.03	1044.9	0.054
3	A/W=72%	322.86	1081.22	2962.96	0.216
4	A/W=72%	315.39	1085.77	2941.89	0.216
5	A/W=72%	315.92	3017.4	2970.83	0.216
6	A/W=72%	349.97	2984.82	2927.82	0.216
7	A/W=72%	368.25	2984.74	2964.84	0.216
8	A/W=59%	370.01	3029.55	1895.55	0.162
9	A/W=59%	324.26	2992.64	1923.22	0.162
10	A/W=59%	380.09	1089.3	1783.68	0.162
11	CH_4= 90.4%, C_2H_6= 5.4%, C_3H_8= 4.0%, N_2= 0.2%	111.25	100.35	21489.47	0.082
12	CH_4= 90.4%, C_2H_6= 5.4%, C_3H_8= 4.0%, N_2= 0.2%	111.18	1214.85	21539.29	0.082
13	CH_4= 90.4%, C_2H_6= 5.4%, C_3H_8= 4.0%, N_2= 0.2%	295.71	1196.34	21803.44	0.082
14	CH_4= 90.4%, C_2H_6= 5.4%, C_3H_8= 4.0%, N_2= 0.2%	242.44	448.3	21728.43	0.082
15	CH_4= 90.4%, C_2H_6= 5.4%, C_3H_8= 4.0%, N_2= 0.2%	282.23	453.29	21784.89	0.082
16	FWS=36,861ppm	320.54	100.85	11.99	10.56
17	FWS=36,861ppm	320.54	645.59	13.43	10.56
18	FWS=36,861ppm	320.54	627.73	30.26	10.56
19	FWS=36,861ppm	320.54	603.71	30.26	10.56
20	FWS=36,861ppm	320.54	6055.45	30.26	10.56
21	FWS=36,861ppm	320.54	629.76	34.45	0.018
22	FWS=36,861ppm	320.54	178.41	42.79	0.018
23	Desalinated water 350 ppm	320.54	180.16	44.85	6.778
24	Brine water 81,250 ppm	320.54	5065.09	48.99	3.781
25	Brine water 81,250 ppm	320.54	100.48	53	3.781
26	Freshwater 450 ppm	320.54	179.36	11.99	6.796
27	Freshwater 450 ppm	320.54	100.78	13.43	6.796
28	FWS=34,850 ppm	298.04	101.77	0	11.248
29	FWS=34,850 ppm	329.69	100.71	20.6	11.248
30	FWS=34,850 ppm	352.42	101.95	56.14	11.248
31	RO feedwater 36,861 ppm	320.54	100.85	8.94	10.56
32	Humid air, ω_a = 93%	334.28	101.75	35.9	4.808
33	Humid air, ω_a = 93%	313.21	101.8	2.1	4.808
34	Pure water	324.13	101.66	1.17	0.562
TOTAL	brine water 44,327 ppm	315.28	100.52	1	3.781
TOTAL	freshwater 356 ppm	297.69	101.36	1	7.358

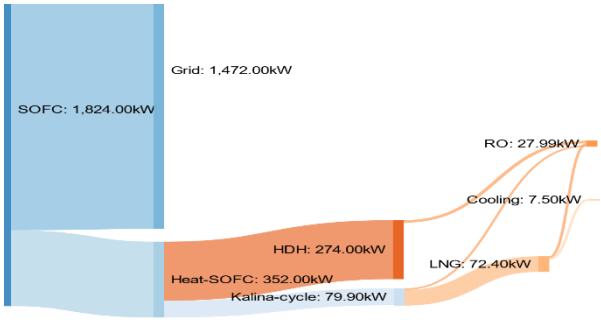

Fig. 3: Energy flow diagram

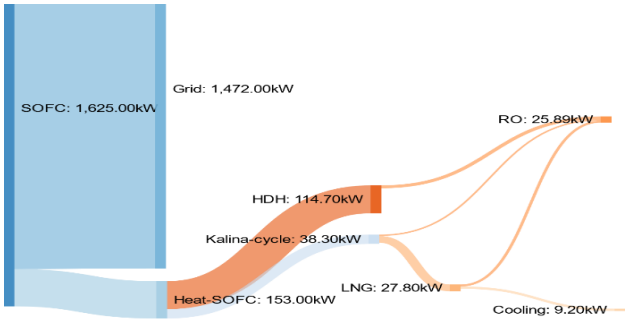

Fig. 4: Exergy flow diagram

Figs. 3 and 4 show the exergy and energy flow of the subsystems.

Figs. 5 and 6 presets the exergy destruction for different parts of the system in the aforementioned

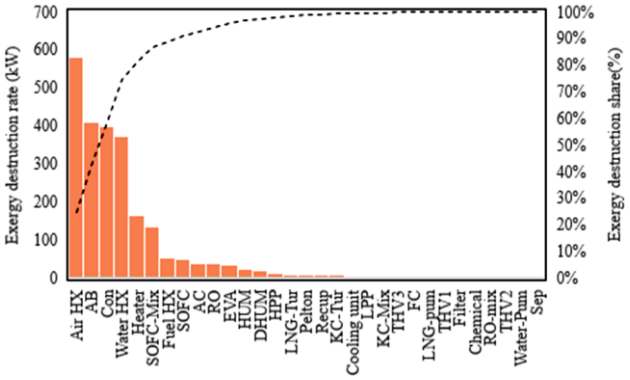

Fig. 5: Exergy destruction rate of each component in system

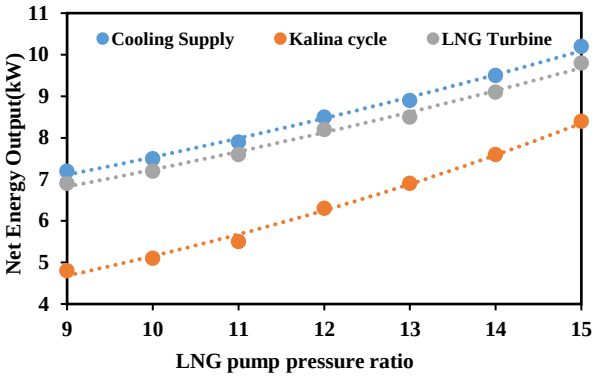

Fig. 8: Water production to Exergy destruction of RO-HDH ratio in different LPP Pressure ratio

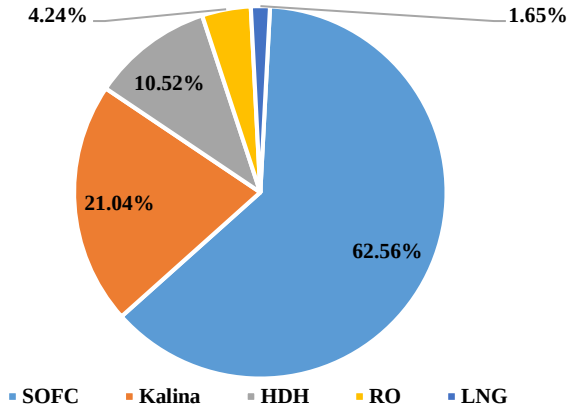

Fig. 6: Exergy destruction of each subsystem in plant

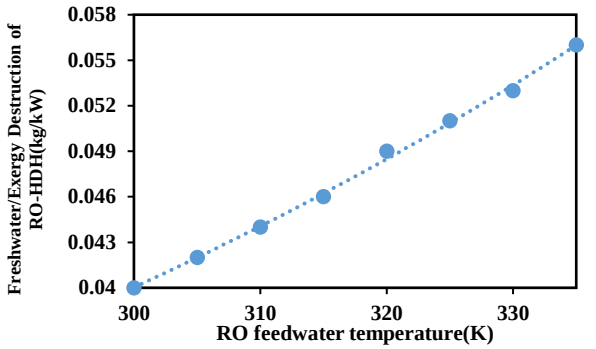

Fig. 9: Water production to Exergy destruction of RO-HDH ratio in different RO feedwater temperature

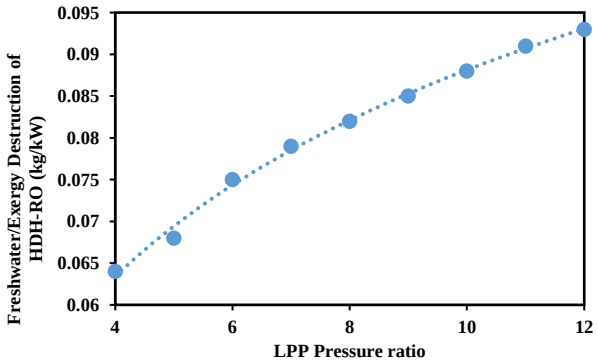

Fig. 7. Net energy output of each subsystem in different LNG pump pressure ratio

configurations. The highest total exergy destruction was observed in the system with LNG system. Then Kalina cycle, while for the water preheating case, the most destruction was detected in the collector. The collector and humidifier exhibited the highest exergy destruction for the air-water preheating case.

Fig. 8 shows the effect of humidifier inlet water temperature on the humidification exergy efficiency for the three studied configurations. It can be easily concluded that exergy efficiency increased with the inlet water temperature of the humidifier. This behavior could be due to the higher vapor absorption ability at higher temperatures. Moreover, exergy efficiency in the air preheating case was lower than in the other cases.

Fig. 10 shows the actual voltage changes of the fuel cell with current density. Increasing the current density reduces the actual voltage due to all the voltage drops inside the fuel cell. Fig. 11 shows the effect of the change in current density on the cycle's net power and the Gax cycle's cooling cycle. By increasing the current density and decreasing voltage, the production capacity of the fuel cell increases. On the other hand, the amount of hydrogen consumption in the fuel cell increases, and as a result, the flow of fuel and air entering the cycle and the power consumption of the compressors and the production capacity of the gas turbine increase. Finally, according to Fig. 5, the net output power of the cycle increases. Due to the increase in temperature and flow of turbine exhaust

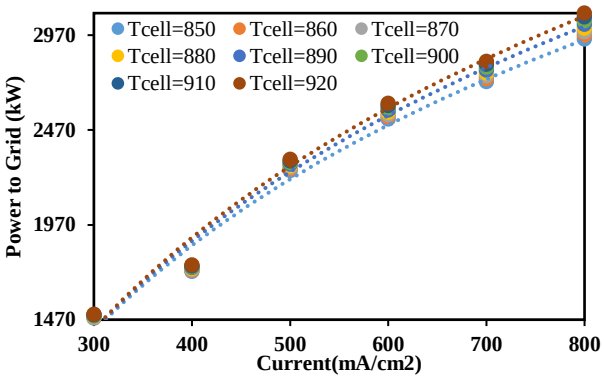

Fig. 10: Power to grid in different SOFC operting temperatures (in K) and currents (mA/cm^2)

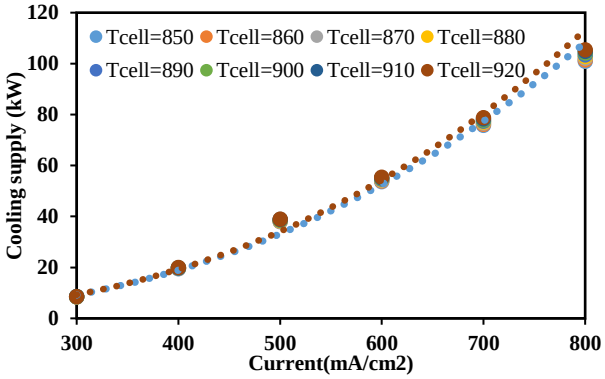

Fig. 12. Cooling Supply in different SOFC operting temperatures (in K) and currents (mA/cm^2)

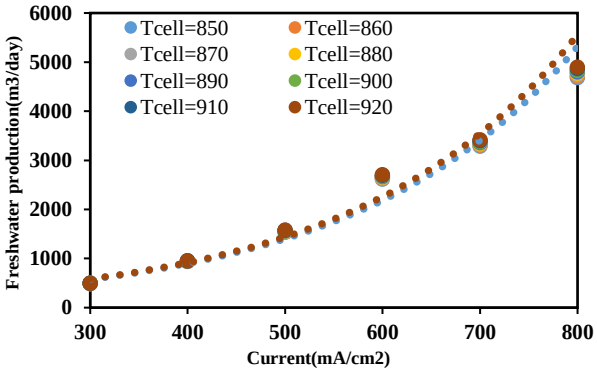

Fig. 11: Feedwater in different SOFC operting temperatures (in K) and currents (mA/cm^2)

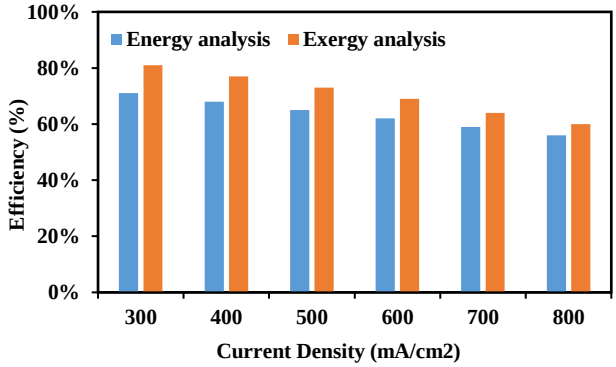

Fig. 13: Exergy and Energy efficiency in different SOFC operting current density

gases, the amount of refrigeration produced in the evaporator increases. The energy efficiency changes of the proposed cycle with the current density are plotted in Figs. 12 and 13. According to this Fig., the cycle efficiency increases as the current density increases.

Increasing the current density reduces the SOFC efficiency, which ultimately reduces the total cycle exergy efficiency. Besides, the increase in current density is accompanied by an increase in the fuel flow inlet to the fuel cell, which increases the mass flow rate of the smoke entering the HRSG, so as shown in Fig. (12), with increasing current density, the mass flow of steam Also increases.

CONCLUSIONS

This paper introduces a new combined cycle for simultaneous electric power-refrigeration production by combining solid oxide fuel cells with the Gax adsorption refrigeration cycle. After reviewing the results of modeling this cycle, the following items can be presented as summarizing the work. By adding the gas cycle to the solid oxide-gas turbine fuel cell system, the heat output of the gas turbine exhaust gases can be used to produce refrigeration so that the combined cycle's energy efficiency increases significantly compared to the simple fuel cell cycle. As the current density increases, the net power of the cycle, the production coldness, and the flow rate of the input fuel to the cycle increase simultaneously, so that due to the greater increase in the useful output of the cycle, the energy efficiency increases with increasing current density. Increasing the operating temperature of the fuel cell causes the cycle efficiency to decrease first and then increase. Despite the increasing ambient temperature, the combined cycle's energy efficiency increases despite the decrease in system production capacity.

Nomenclature

FCG	Fuel cell group
SOFC	solid oxide fuel cell

AC	Air compressor
FC	Fuel compressor
WP	Water pump
AP	Air preheater
FP	Fuel preheater
WP	Water preheater
Mix	Mixer
AB	Afterburner
KC	Kalina cycle
EVA	Evaporator
SEP	Separator
TUR	Turbine
RECUP	Recuperator
THV	Throttle valve
MED	Multi-Effect Desalination
GT	Gas Turbine
W_{SOFC}	Output power of SOFC (W)
V_{loss}	Voltage losses (V)
V_{cell}	Cell's voltage (V)
V_N	Reversible voltage (V)
A_{act}	Activation area (m^2)
ζ_{conc}	Concentration overpotential (V)
ex	Exergy(Kw)
m	Mass flow(kg/s)
X	Mass fraction
T	Temperature(K)
h	Enthalpy (kJ/kg)
s	Entropy (kJ/kg.K)
t	Thickness (m)
an	anode
ca	cathode
exc	exchange
ele	Electrolyte
int	Interconnect
S/C	Steam-to-carbon ratio
FWS	Feedwater salinity (ppm)
ω	Relative humidity (%)
W/A	Water-to-air mass flow ratio
Pum	Pump
WH	Water heater
LNGC	LNG cooling
CU	Cooling unit
HDH	humidification-dehumidification
HUM	Humidifier
DHUM	Dehumidifier
ROM	RO module
LPP	Low pressure pump
HPP	high pressure pump
PTu	Pelton turbine
LNG	Liquefied natural gas
GOR	gained output ratio
RO	Reverse osmosis
TEG	Thermoelectric generator
PEMFC	Proton Exchange Membrane Fuel Cell
OWCA	Open Water Close Air
CPVT	Concentrated Photovoltaic Thermal
y_s	Mass fraction of salt
R_r	Recovery ratio
N_{cell}	Number of cells
i	Current density (A/m^2)
ζ_{ohm}	Ohmic overpotential (V)
ζ_{act}	Activation overpotential (V)
ph	physical
ch	chemical
Q	Heat (kW)
P	Pressure(kPa)
FUF	Fuel utilization factor (%)
N_e	Number of electrons
Dif	Effective gaseous diffusivity (m^2/s)
η	Efficiency
ΔP	Pressure drop (%)
HX	Heat exchanger
r	Pump pressure ratio
PPTD	Pinch point temperature difference (K)
TTD	Terminal temperature difference (K)
A/W	Ammonia-water mass fraction
RRO	Recovery ratio of RO unit
MSR	Membrane salt rejection ratio

Received :Sep. 18, 2022 ; Accepted : May. 01, 2023

REFERENCES

[1] Zhu J., Hu K., Lu X., Huang X., Liu K., Wu X., A Review of Geothermal Energy Resources Development, and Applications in China: Current Status and Prospects, *Energy*, **93**: 466-483 (2015).

[2] Alhamid M.I., Daud Y., Surachman A., Sugiyono A., Aditya H.B., Mahlia T.M., Potential of Geothermal Energy for Electricity Generation in Indonesia: A Review, *Renewable and Sustainable Energy Reviews*, **53**:733-40 (2016).

[3] Michaelides E.E., Future Directions and Cycles for Electricity Production from Geothermal Resources, *Energy Conversion and Management*, **107**:3-9 (2016).

[4] Wu C., Wang S.S., Li J., Exergoeconomic Analysis and Optimization of a Combined Supercritical Carbon Dioxide Recompression Brayton/Organic Flash Cycle for Nuclear Power Plants, *Energy Conversion and Management*, **171**:936-52 (2018).

[5] Hsieh J.C., Lee Y.R., Guo T.R., Liu L.W., Cheng P.Y., Wang C.C., A Co-Axial Multi-Tube Heat Exchanger Applicable for a Geothermal ORC Power Plant, *Energy Procedia*, **61**:874-7 (2014).

[6] Astolfi M., Romano M.C., Bombarda P., Macchi E., Binary ORC (Organic Rankine Cycles) Power Plants for the Exploitation of Medium–Low Temperature Geothermal Sources–Part B: Techno-Economic Optimization, *Energy*, **66**:435-46 (2014).

[7] Zhai H., Shi L., An Q., Influence of Working Fluid Properties on System Performance and Screen Evaluation Indicators for Geothermal ORC (Organic Rankine Cycle) System, *Energy*, **74**:2-11 (2014).

[8] Orhan M.F., Babu B.S., Investigation of An Integrated Hydrogen Production System Based on Nuclear and Renewable Energy Sources: Comparative Evaluation of Hydrogen Production Options With a Regenerative Fuel Cell System, *Energy*, **88**:801-20 (2015).

[9] Zhong J., Stevens D.K., Hansen C.L., Optimization of Anaerobic Hydrogen and Methane Production from Dairy Processing Waste Using a Two-Stage Digestion in Induced Bed Reactors (IBR), *International Journal of Hydrogen Energy*, **40(45)**:15470-6 (2015).

[10] Monfort O., Pop L.C., Sfaelou S., Plecenik T., Roch T., Dracopoulos V., Stathatos E., Plesch G., Lianos P., Photoelectrocatalytic Hydrogen Production by Water Splitting Using $BiVO_4$ Photoanodes, *Chemical Engineering Journal*, **286**: 91-7 (2016).

[11] Dincer I., Green Methods for Hydrogen Production, *International Journal of Hydrogen Energy*, **37(2)**:1954-71 (2012).

[12] Caliskan H., Dincer I., Hepbasli A., Energy, Exergy and Sustainability Analyses of Hybrid Renewable Energy Based Hydrogen and Electricity Production and Storage Systems: Modeling and Case Study, *Applied Thermal Engineering*, **61(2)**: 784-98 (2013).

[13] Pham A.T., Baba T., Shudo T., Efficient Hydrogen Production from Aqueous Methanol in a PEM Electrolyzer with Porous Metal Flow Field: Influence of Change in Grain Diameter and Material of Porous Metal Flow Field, *International Journal of Hydrogen Energy*, **38(24)**: 9945-53 (2013).

[14] Ratlamwala T.A., Dincer I., Comparative Efficiency Assessment of Novel Multi-Flash Integrated Geothermal Systems for Power and Hydrogen Production, *Applied Thermal Engineering*, **48**: 359-66 (2012).

[15] Cao Y., Haghghi M.A., Shamsaiee M., Athari H., Ghaemi M, Rosen M.A., Evaluation and Optimization of a Novel Geothermal-Driven Hydrogen Production System Using an Electrolyser Fed by a Two-Stage Organic Rankine Cycle with Different Working Fluids, *Journal of Energy Storage*, **32**: 101766 (2020).

[16] Atalay H., Comparative Assessment of Solar and Heat Pump Dryers with Regards to Exergy and Exergoeconomic Performance, *Energy*, **189**:116180 (2019).

[17] Norouzi N., Fani M., Talebi S., Exergetic Design and Analysis of a Nuclear SMR Reactor Tetrageneration (Combined Water, Heat, Power, and Chemicals) with Designed PCM Energy Storage and a CO_2 Gas Turbine Inner Cycle, *Nuclear Engineering and Technology*, **53(2)**:677-87 (2021).

[18] Yuksel Y.E., Ozturk M., Thermodynamic and Thermoeconomic Analyses of a Geothermal Energy Based Integrated System for Hydrogen Production, *International Journal of Hydrogen Energy*, **42**: 2530-46 (2017).

[19] Norouzi N., Talebi S., Fani M., Khajehpour H., Exergy and Exergoeconomic Analysis of Hydrogen and Power Cogeneration Using an HTR Plant, *Nuclear Engineering and Technology*, **53**: 2753-2760 (2021).

[20] Balta M.T., Dincer I., Hepbasli A., Exergoeconomic Analysis of a Hybrid Copper–Chlorine Cycle Driven by Geothermal Energy for Hydrogen Production, *International Journal of Hydrogen Energy*, **36(17)**: 11300-8 (2011).

[21] Cai Q., Adjiman C.S., Brandon N.P., Optimal Control Strategies for Hydrogen Production When Coupling Solid Oxide Electrolysers with Intermittent Renewable Energies, *Journal of Power Sources*, **268**: 212-24 (2014).

[22] Ouali S., Chader S., Belhamel M., Benziada M., The Exploitation of Hydrogen Sulfide for Hydrogen Production in Geothermal Areas, *International Journal of Hydrogen Energy*, **36(6)**: 4103-9 (2011).

[23] Mahmoud M., Ramadan M., Naher S., Pullen K., Abdelkareem M.A., Olabi A.G., A Review of Geothermal Energy-Driven Hydrogen Production Systems, *Thermal Science and Engineering Progress*, **22**: 100854 (2021).

[24] Parham K, Assadi M., A Parametric Performance Analysis of a Novel Geothermal Based Cogeneration System, *Sustainable Energy Technology and Policies*, 167-182 (2018).

[25] Han J., Wang X., Xu J., Yi N., Talesh S.S., Thermodynamic Analysis and Optimization of an Innovative Geothermal-Based Organic Rankine Cycle Using Zeotropic Mixtures for Power and Hydrogen Production, *International Journal of Hydrogen Energy*, **45(15)**: 8282-99 (2020).

[26] Yuksel Y.E., Ozturk M., Dincer I., Energetic and Exergetic Performance Evaluations of a Geothermal Power Plant Based Integrated System for Hydrogen Production, *International Journal of Hydrogen Energy*, **43(1)**: 78-90 (2018).

[27] Cao Y., Dhahad H.A., Togun H., Hussen H.M., Rashid T.A., Anqi A.E., Farouk N., Issakhov A., Exergetic and Financial Parametric Analyses and Multi-Objective Optimization of a Novel Geothermal-Driven Cogeneration Plant; Adopting a Modified Dual Binary Technique, *Sustainable Energy Technologies and Assessments*, **48**: 101442 (2021).

[28] Cao L., Lou J., Wang J., Dai Y., Exergy Analysis and Optimization of a Combined Cooling and Power System Driven by Geothermal Energy for Ice-Making and Hydrogen Production, *Energy Conversion and Management*, **174**: 886-96 (2018).

[29] Yilmaz C., Koyuncu I., Alcin M., Tuna M., Artificial Neural Networks Based Thermodynamic And Economic Analysis of a Hydrogen Production System Assisted by Geothermal Energy on Field Programmable Gate Array, *International Journal of Hydrogen Energy*, **44(33)**: 17443-59 (2019).

[30] Talebi S., Norouzi N., Entropy and Exergy Analysis and Optimization of the VVER Nuclear Power Plant With a Capacity of 1000 MW Using the Firefly Optimization Algorithm, *Nuclear Engineering and Technology*, **52(12)**: 2928-38 (2020).

[31] Norouzi N., 4E Analysis of a Fuel Cell and Gas Turbine Hybrid Energy System, *Biointerface Res. Appl. Chem.*, **11**: 7568-7579(2021).

[32] Norouzi N., Talebi S., Exergy and Energy Analysis of Effective Utilization of Carbon Dioxide in the Gas-to-Methanol Process, *Iranian Journal of Hydrogen & Fuel Cell*, **7(1)**: 13-31(2020).

[33] Norouzi N., 4E Analysis and Design of a Combined Cycle with a Geothermal Condensing System in Iranian Moghan Diesel Power Plant, *International Journal of Air-Conditioning and Refrigeration*, **28**: 2050022 (2020).

[34] Algieri A., Morrone P., Energetic Analysis of Biomass-Fired ORC Systems for Micro-Scale Combined Heat And Power (CHP) Generation. A Possible Application to the Italian Residential Sector, *Applied Thermal Engineering*, **71(2)**: 751-9 (2014).

[35] Lee J., Hong S., Cho H., Lyu B., Kim M., Kim J., Moon I., Machine Learning-Based Energy Optimization for on-Site Smr Hydrogen Production, *Energy Conversion and Management*, **244**: 114438 (2021).

[36] Norouzi N., Hosseinpour M., Talebi S., Fani M., A 4E Analysis of Renewable Formic Acid Synthesis from the Electrochemical Reduction of Carbon Dioxide and Water: Studying Impacts of the Anolyte Material on the Performance of the Process, *Journal of Cleaner Production*, **293**: 126149 (2021).

[37] Wang J., Yan Z., Wang M., Ma S., Dai Y., Thermodynamic Analysis and Optimization of an (Organic Rankine Cycle) ORC Using Low Grade Heat Source, *Energy*, **49**: 356-65 (2013).

[38] Leveni M., Manfrida G., Cozzolino R., Mendecka B., Energy and Exergy Analysis of Cold and Power Production from the Geothermal Reservoir of Torre Alfina, *Energy*, **180**: 807-18 (2019).

[39] Norouzi N., Kalantari G., Talebi S., Combination of Renewable Energy in the Refinery, with Carbon Emissions Approach, *Biointerface Res. Appl. Chem.*, **10(4)**: 5780-6(2020).

[40] Norouzi N., Talebi S., Najafi P., Thermal-Hydraulic Efficiency of a Modular Reactor Power Plant by Using the Second Law of Thermodynamic, *Annals of Nuclear Energy*, **151**: 107936 (2021).

[41] Khajehpour H., Norouzi N., Shiva N., Folourdi R.M., Bahremani E.H., Exergy Analysis and Optimization of Natural Gas Liquids Recovery Unit, *International Journal of Air-Conditioning and Refrigeration*, **29**: 2150005 (2021).

[42] Khajehpour H., Norouzi N., Bashash Jafarabadi Z., Valizadeh G., Hemmati M.H., Energy, Exergy, and Exergoeconomic (3E) Analysis of Gas Liquefaction and Gas Associated Liquids Recovery Co-Process Based on the Mixed Fluid Cascade Refrigeration Systems, *Iranian Journal of Chemistry and Chemical Engineering (IJCCE)*, **41(4)**: 1391-1410 (2022).

[43] Norouzi N., Thermodynamic and Irreversibility Analysis of the Use of Hydrogen for the Energy Conversion of Fossil Fuel in Power Plants, *Journal of Applied Dynamic Systems and Control*, **4(1)**: 97-107 (2021).

[44] Norouzi N., Technical and Economic and Exergy Feasibility of Combined Production of Electricity and Hydrogen Using Photovoltaic Energy, *Journal of Applied Dynamic Systems and Control*, **4(1)**: 79-88 (2021).

[45] Ahmed S., Lee S.H., Ferrandon M.S., Catalytic Steam Reforming of Biogas–Effects of Feed Composition and Operating Conditions, *International Journal of Hydrogen Energy*, **40(2)**: 1005-15 (2015).

[46] Bazregari M.J., Gholinejad M., Peydayesh Y., Norouzi N., Fani M., Exergoeconomic Analysis of the Cycle of Cogeneration of Power, Cooling and Freshwater for a Residential Complex in Iran, *International Journal of Air-Conditioning and Refrigeration*, 2150030 (2021).

[47] Norouzi N., Talebi S., Exergy, Economical and Environmental Analysis of a Natural Gas Direct Chemical Looping Carbon Capture and Formic Acid-Based Hydrogen Storage System, *Iranian Journal of Chemistry and Chemical Engineering (IJCCE)*, **41(4)**: 1436-1457 (2021).

[48] Bazregari M.J., Norouzi N., Gholinejad M., Khavasi E., Fani M., A 2E Analysis and Optimization of a Hybrid Solar Humidification-Dehumidification Water Desalination System and Solar Water Heater, *Iranian Journal of Chemistry and Chemical Engineering (IJCCE)*, **41(6)**: 2135-2152 (2022).

[49] Norouzi N., Fani M., Energy and Exergy Analysis and Selection of the Appropriate Operating Fluid for a Combined Power and Hydrogen Production System Using a Geothermal Fueled ORC and a PEM Electrolyzer, *Iranian Journal of Chemistry and Chemical Engineering (IJCCE)*, **41(5)**: 1786-1802 (2022).

[50] Norouzi N., Hydrogen Production in the Light of Sustainability: A Comparative Study on the Hydrogen Production Technologies Using the Sustainability Index Assessment Method, *Nuclear Engineering and Technology*, (2021).

[51] Mohammadi A., Ahmadi M. H., Bidi M., Joda F., Valero A., Uson S., Exergy Analysis of a Combined Cooling, Heating and Power System Integrated with Wind Turbine and Compressed Air Energy Storage System, *Energy Conversion and Management*, **131**: 69-78 (2017).

[52] Mohammadi A., Kasaeian A., Pourfayaz F., Ahmadi M. H., Thermodynamic Analysis of a Combined Gas Turbine, ORC Cycle and Absorption Refrigeration for a CCHP System, *Applied Thermal Engineering*, **111**: 397-406 (2017).

[53] Naseri A., Bidi M., Ahmadi M. H., Saidur R., Exergy Analysis of a Hydrogen and Water Production Process by a Solar-Driven Transcritical CO_2 Power Cycle with Stirling Engine, *Journal of Cleaner Production*, **158**: 165-181 (2017).

[54] Naseri A., Bidi M., Ahmadi M.H., Thermodynamic and Exergy Analysis of a Hydrogen and Permeate Water Production Process by a Solar-Driven Transcritical CO_2 Power Cycle with Liquefied Natural Gas Heat Sink, *Renewable Energy*, **113**: 1215-1228 (2017).

[55] Naseri A., Fazlikhani M., Sadeghzadeh M., Naeimi A., Bidi M., Tabatabaei S.H., Thermodynamic and Exergy Analyses of a Novel Solar-Powered CO_2 Transcritical Power Cycle with Recovery of Cryogenic LNG Using Stirling Engines, *Renewable Energy Research and Applications*, **1(2)**: 175-185 (2020).

[56] Raei B., Ghadi A., Bozorgian A., "Heat Integration of Heat Exchangers Network Using Pinch Technology", in: *19th International Congress of Chemical and Process Engineering CHISA*, (2010)

[57] Pourabadeh A., Nasrollahzadeh B., Razavi R., Bozorgian A., Najafi M., A.Oxidation of FO and N2 Molecules on the Surfaces of Metal-Adopted Boron Nitride Nanostructures as Efficient Catalysts, *J. Struct. Chem*., **59**: 1484–1491 (2018).

[58] Esmaeili Bidhendi M., Asadi Z., Bozorgian A., et al., New Magnetic Co3O4/Fe3O4 Doped Polyaniline Nanocomposite for the Effective and Rapid Removal of Nitrate Ions from Ground Water Samples, *Environ. Prog. Sustainable Energy.*, **39**: e13306 (2019).

[60] Bozorgian A., Arab Aboosadi Z., Mohammadi A., Honarvar B., Azimi A., Optimization of Determination of CO2 Gas Hydrates Surface Tension in the Presence of Non-Ionic Surfactants and TBAC, *Eurasian Chem. Commun.*, **2**: 420-426 (2020).

[61] Mashhadizadeh J., Bozorgian A., Azimi A., Investigation of the Kinetics of Formation of Clatrit-Like Dual Hydrates TBAC in the Presence of CTAB, *Eurasian Chem. Commun.*, **2**: 536-547 (2020).

[62] Norouzi N., Bozorgian A., Dehghani M., Best Option of Investment in Renewable Energy: A Multicriteria Decision-Making Analysis for Iranian Energy Industry, *Journal of Environmental Assessment Policy and Management*, **22**: No. 01n02, 2250001 (2020).

[63] Norouzi N., Ebadi A., Bozorgian A., Hoseyni S.J., Vessally E., Energy and Exergy Analysis of Internal Combustion Engine Performance of Spark Ignition for Gasoline, Methane, and Hydrogen Fuels, *Iran. J. Chem. Chem. Eng. (IJCCE)*, **40(6)**: 1909-1930 (2021).

[64] Bozorgian A., Arab Aboosadi Z., Mohammadi A., Honarvar B., Azimi A., Statistical Analysis of the Effects of Aluminum Oxide (Al_2O_3) Nanoparticle, TBAC, and APG on Storage Capacity of CO_2 Hydrate Formation, *Iran. J. Chem. Chem. Eng. (IJCCE)*, **41(1)**: 220-231 (2022).

[65] Ahmadpour A., Bozorgian A., Eslamimanesh A., Mohammadi A.H., Photocatalytic Treatment of Spontaneous Effluent of Petrochemical Effluents by TiO_2 CTAB Synthetic Nanoparticles, *Desalin. Water Treat.*, 249: 297-308 (2022).

[66] Norouzi N., Ebadi A., Bozorgian A., Hoseyni S.J., Vessally E., Cogeneration System of Power, Cooling, and Hydrogen from Geothermal Energy: An Exergy Approach, *Iran. J. Chem. Chem. Eng. (IJCCE)*, **41(2)**: 706-721 (2022).

[67] Bozorgian A., Arab Aboosadi Z., Mohammadi A., Honarvar B., Azimi A., Determination Of CO_2 Gas Hydrates Surface Tension in the Presence of Nonionic Surfactants and TBAC, *Rev. Roum. Chim.*, **65**: 1061-1065 (2020).

[68] Kanani M., Kanani N., Batooie N., Bozorgian A., Barghi A., Rezania Sh., Removal of Rhodamine 6G Dye Using One-Pot Synthesis of Magnetic Manganese Graphene Oxide: Optimization by Response Surface Methodology, *Environ. Nanotechnol., Monit. Manage.*, **18**: 100709 (2022).